Retinal Regeneration Following OCT-Guided Laser Injury in Zebrafish

Rose M. DiCicco, Brent A. Bell, Charles Kaul, Joe G. Hollyfield, Bela Anand-Apte, Brian D. Perkins, Yuankai K. Tao, and Alex Yuan

Cole Eye Institute, Cleveland Clinic, Cleveland, Ohio, United States

Correspondence: Alex Yuan, Cleveland Clinic, 9500 Euclid Avenue, i32, Cleveland, OH 44195, USA yuana@ccf.org.

RMD and BAB contributed equally to the work presented here and should therefore be regarded as equivalent authors.

Submitted: May 3, 2014
Accepted: August 28, 2014

Citation: DiCicco RM, Bell BA, Kaul C, et al. Retinal regeneration following OCT-guided laser injury in zebrafish. *Invest Ophthalmol Vis Sci*. 2014;55:6281–6288. DOI:10.1167/iovs.14-14724

Purpose. Establish a focal injury/regeneration model in zebrafish using laser photocoagulation guided by optical coherence tomography (OCT).

Methods. Adult zebrafish were imaged by OCT and confocal scanning laser ophthalmoscopy (cSLO) in room air through a contact lens. Using a beam combiner, 532-nm laser photocoagulation was applied using the OCT C-scan image for targeting. Laser spots of 42 to 47 mW were delivered to the retina. At multiple intervals post injury, fish were imaged using both OCT and cSLO to follow the progression of each lesion. Histologic sections and TUNEL staining were performed to monitor the injury response.

Results. Round lesions (26057 ± 621 μm^2) localized to the outer retina were successfully applied. Laser application was visualized by real-time OCT and lesions were detectable by both OCT and cSLO in vivo. Lesion size increased 1 day post lesion then decreased in size. Histologic sections showed focal areas of damage localized primarily to the outer retina. By 3 weeks, the damaged areas had regenerated and a fully laminated structure was re-established. However, subtle changes can still be detected by OCT, cSLO imaging, and histology. Infrared darkfield imaging was more sensitive than OCT at revealing subtle changes in regenerated areas.

Conclusions. Optical coherence tomography–guided laser photocoagulation is a useful tool for inducing localized lesions and studying retinal regeneration in zebrafish. This novel method will allow us to characterize the cellular and molecular changes that take place at the interface between normal and damaged tissue. Regeneration can be observed using high-resolution OCT and cSLO imaging in vivo.

Keywords: regeneration, scanning laser ophthalmoscopy, optical coherence tomography, laser, retina

The zebrafish retina is capable of regeneration in response to damage from intense light,[1] cytotoxin,[2] mechanical,[3] and thermal injury.[4] All of these mechanisms of injury result in relatively large lesions or damage to the entire retina and other ocular structures. Recently, focused light has been used to damage the retina.[5] Although the lesions are much more localized in this model, there are multiple zones of damage produced as well as variability in the degree of damage within each zone. A method to produce a focal lesion disrupting the outer retina with minimal collateral damage has not been developed for zebrafish. The purpose of this study is to describe an optical coherence tomography (OCT)-guided laser photocoagulation model of retinal regeneration in zebrafish. Our model produced consistent focal damage to the outer retina and allowed us to monitor each lesion in vivo as they regenerated, using both OCT and confocal scanning laser ophthalmoscopy (cSLO). Laser injury in our model occurred in less than 1 second, which could allow for the precise timing of molecular and cellular events during regeneration.

Optical coherence tomography imaging produces high-resolution, cross-sectional images of the retina, providing information, which was previously only available with histology.[6] The image is produced by light reflected and backscattered by different layers of the retina. This generates different banding patterns on OCT, which correspond to the various retinal layers. Damage to different retinal layers can be monitored by examining the banding pattern changes on OCT. Optical coherence tomography allows for noninvasive imaging through a small pupil, and produces both high-resolution, cross-sectional images (B scan) and en face images (C scan). Disadvantages include the inability to image through opaque media, the inability to image the periphery, the inability to detect labeled cells by OCT, and limitations on imaging speed. Optical coherence tomography imaging of zebrafish has been previously described for the whole eye,[7,8] and more recently in a transpupillary fashion in the adult zebrafish retina.[5,9]

Confocal scanning laser ophthalmoscopy imaging uses a laser instead of white light to illuminate the retina and produces images from reflected light or fluorescence. The light passes through a confocal pinhole to narrow the depth of focus and increase the clarity of the image. By using a confocal pinhole, the stray light outside of the focal plane is excluded, thereby producing a high-resolution image of a thin optical plane of the retina.[10] Advantages include a noninvasive method of imaging the retina through a small pupil, the ability to detect fluorescent-labeled cells (and autofluorescence [AF]), and the rapid acquisition speed. Disadvantages include the inability to image through opaque media and inability to image the far

peripheral retina. Although cSLO imaging of zebrafish retina has been previously reported at a meeting,[11] those images would not be of sufficient resolution to monitor laser lesions. More recently, high-resolution images of the zebrafish retina has been successfully obtained in a transpupillary fashion (Bell BA, Xie J, Yuan A, Kaul C, Hollyfield JG, Anand-Apte B, manuscript submitted, 2014). Our technique not only enables us to monitor regeneration in vivo, but we found it to be more sensitive than OCT and histology at revealing subtle changes to the retinal architecture following laser injury and retinal regeneration in zebrafish.

In this report, we describe a novel method of focal injury using a laser targeted by OCT. Using this method of retinal injury on adult zebrafish, we were able to monitor the injury and subsequent regeneration in vivo by OCT and cSLO imaging. Focal injury is advantageous for studying certain biological processes such as the migration of cells in response to injury, the response at the marginal zone where normal retina is adjacent to injured retina, and the precise timing of events that take place during retinal regeneration.

Methods

Protocol approval by the Cleveland Clinic Institutional Animal Care and Use Committee (Cleveland, OH, USA) was obtained and all studies conformed to the ARVO Statement for the Use of Animals in Ophthalmic and Vision Research.

Anesthesia

Adult wildtype zebrafish between the ages of 4 months to 1 year were placed in 0.12 to 0.17 mg/mL tricaine (Acros Organics, Morris Plains, NJ, USA) solution until they became immobile and did not respond to external stimuli. Each fish was transferred to a custom rubber mat for imaging.

Imaging

The zebrafish eye has a spherical lens with very high diopteric power and a flattened cornea compared with humans. The optics are optimized for aquatic environments, and thus a poly methyl methacrylate (PMMA) contact lens (Ø = 5.2 mm, r = 2.70 mm, center thickness = 0.4 mm; Cantor & Nissell, Ltd., Northamptonshire, UK) is necessary for optimal images. The concave surface was placed over the eye using Systane Ultra hydrating tears (Alcon Laboratories, Fort Worth, TX, USA). Standard cSLO (HRA2; Heidelberg Engineering, Carlsbad, CA, USA) and OCT (SDOIS 840HR; Bioptigen, Durham, NC, USA) systems equipped with wide-field objectives (≥50° field of view) were used. The OCT system has an axial resolution of 7 μm. For each animal, cSLO images were acquired prior to OCT images. Images were obtained in both AF and reflectance modes, and were performed at several planes of focus. Laser lesion areas were quantitated using ImageJ software (http://imagej.nih.gov/ij/; provided in the public domain by the National Institutes of Health, Bethesda, MD, USA) by outlining the lesion with the freehand tool and using the measurement function. The scale on the cSLO images was calibrated using the optic nerve cross-sectional diameter measured with hematoxylin and eosin (H&E) cryosections. To measure changes in lesion area, ANOVA and Tukey-Kramer HSD tests were performed using JMP 10.0 (SAS, Cary, NC, USA).

Laser Photocoagulation

A 532-nm diode laser (Oculight GL; Iridex, Mountain View, CA, USA) was folded into the OCT-imaging path using a custom-built beam combining module consisting of a dichroic beamsplitter (685-nm long-pass; Semrock, Inc., Rochester, NY, USA), relay optics (Thorlabs, Newton, NJ, USA), and a modified 200-μm multimode optical fiber (Fig. 1). The relay optics allowed for adjustment of the photocoagulation focus to ensure parfocality with the OCT-imaging field. An adjustable aperture was positioned conjugate to the photocoagulation focus. This aperture allowed for titration of energy delivery or lesion size. We set our aperture to a setting of 7.3 mm. The beam combiner allowed for the simultaneous imaging of the retina by OCT and photocoagulation for image-guided laser delivery. The beam combining module allowed OCT and photocoagulation across an approximately 750-μm field of view. The beam combining module was installed prior to laser photocoagulation and was also used to obtain the day 0 images. Otherwise, the standard wide-field objective was used. The module increased the optical length of the OCT imaging system by 1.2 mm, and the reference arm was path-length matched accordingly. Preliminary experiments were performed to determine the optimal duration and power to consistently produce a targeted focal spot on the retina. Prior to each experiment the laser output power was calibrated between 42 and 47 mW. A 300-ms pulse was used for each laser spot. The laser spots were aimed by rotating the animal on a custom, 5-axis positioning stage (Model AIM-RAS; Bioptigen, Inc.) and by using the C-scan image for targeting. Laser spots were placed around the optic nerve. For histologic sections, a row of three laser spots was placed superior to the nerve to facilitate finding the lesions on sectioning. Fish were revived in fish water and were imaged at various intervals between 1 day post lesion (dpl) and 15 weeks post lesion (wpl).

Tissue Processing

Animals were euthanized by rapid submersion in ice water and their eyes were immediately enucleated. The dorsal surface of the zebrafish eye is more darkly pigmented than the ventral surface, thus we used this to aid in orientation. Each eye was snap frozen in optimal cutting temperature compound (Tissue-tek, Torrance, CA, USA) by floating a cryomold cassette (Tissue-tek) in methylbutane (Fisher, Pittsburgh, PA, USA), chilled with liquid nitrogen to approximately −150°C. The eyes were stored at −80°C prior to sectioning. Each eye was mounted to the cryostat such that the ventral surface would be sectioned first. Sections of 10 μm were obtained between −25°C and −28°C using the CryoJane tape transfer system (Leica, Buffalo Grove, IL, USA). All of our laser lesions used for sectioning were placed superior to the optic nerve, thus, we started serial sections dorsal to the optic nerve. This technique allowed us to efficiently identify our laser lesions. For H&E staining, we fixed the sections with 4% paraformaldehyde (EMS, Hatfield, PA, USA) for 10 minutes at 4°C. Sections were then stained with hematoxylin (Fisher) and 0.2% eosin (Fisher) following standard protocols. For TUNEL staining, we followed the manufacturer's recommendations using the In Situ Cell Death Detection kit (Roche, Indianapolis, IN, USA). The cells were counterstained using Vectashield with 4′, 6-diamidino-2-phenylindole (DAPI; Vector Labs, Burlingame, CA, USA). Cell counts were obtained manually using the Leica Application Suite (Leica). Retinal layers were segmented using the position of the nuclear layers to mark the transition between different zones. Three cryosections within 40 μm from the presumed center of each laser lesion were used for cell counts. The sum of cells from these three sections was recorded for each lesion. The mean ± SEM for each time point from three different laser lesions was calculated and plotted using Excel. ANOVA and Tukey-Kramer HSD tests were performed using JMP 10.0.

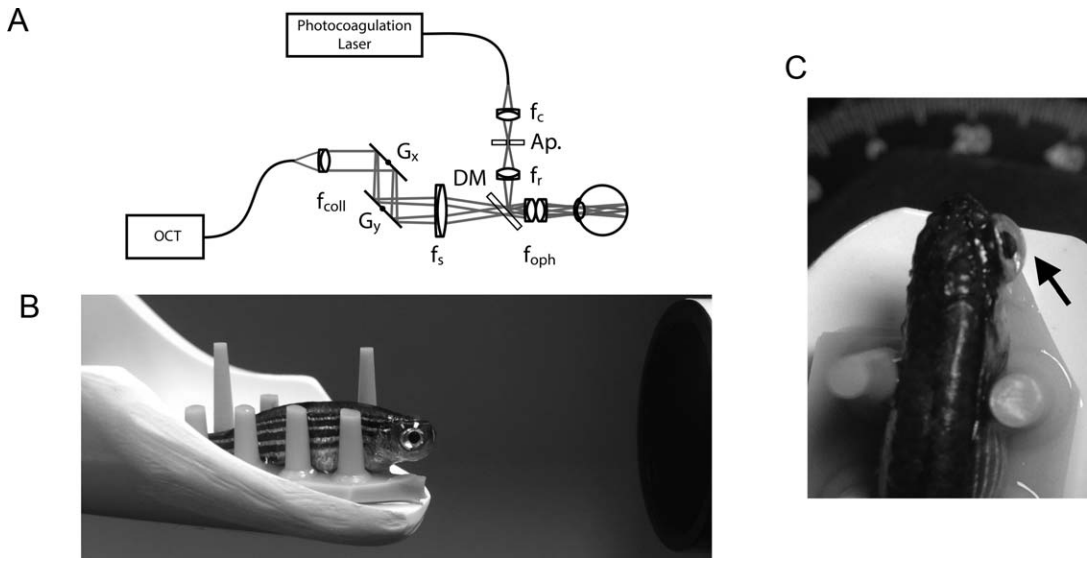

Figure 1. Setup for OCT-guided laser photocoagulation of zebrafish retina. (**A**) Optical schematic of OCT-guided laser system. (**B**) Side view of zebrafish placed on rubber holder with contact lens in place just prior to application of laser. (**C**) Top down view with the *arrow* pointing to the contact lens. Ap, adjustable aperture; DM, dichroic mirror; f_c, collection; f_{coll}, collimating; f_{oph}, ophthalmic; f_r, relay; f_s, scanning lenses; G_x and G_y, two axis scanning mirrors.

Results

In order to obtain images with both OCT and cSLO in room air, a custom contact lens was necessary to compensate for the fish eye optics. Each fish was stabilized on a rubber mat for imaging. Figure 1 shows a schematic of the beam combiner used for laser photocoagulation and examples of fish prepared for imaging. Real-time OCT imaging during laser application (Supplementary Video S1) reveals an immediate increase in hyper-reflectivity localized to the outer retina. Laser lesions can be detected by both OCT and cSLO immediately following application and also on subsequent imaging sessions up to 15 wpl.

On OCT, the lesions were most obvious between 2 and 7 dpl (Figs. 2, 3). Immediately following laser application, a diffuse hyperreflective signal was seen with loss of the outer segment (OS) banding pattern. This diffuse signal became more organized and a dense hyperreflective band was consistently seen at the outer nuclear layer (ONL) extending into the OS bands (Fig. 2). Shadowing was seen below this hyperreflective band with a second outer retinal band at the level of the RPE seen in some animals (Fig. 3, 1 wpl). The OS banding pattern was re-established by 3 wpl in the majority of animals, but a subtle hyperreflective signal remained at the ONL (Fig. 3). This subtle change persisted through 15 wpl.

The timing of changes on cSLO paralleled those seen on OCT with differences at the earliest time points where the cSLO signal was very obvious (Figs. 2, 3). Lesions were visible with both AF and infrared dark field (IRDF) modes. Immediately following laser, the lesions were hyper-AF and quickly became hypo-AF by 1 wpl on AF mode. By 3 to 6 wpl, the lesions were no longer visible (Fig. 3). With IRDF, early lesions exhibited an outer reflective ring surrounding a dark center. This hyperreflective outer ring intensified and migrated centripetally and by 1 wpl, the dark centers became hyperreflective (Figs. 2, 3). There was a significant decrease in average lesion size between each time point until 3 wpl ($P < 0.0001$, ANOVA, Supplementary Material S2). After 3 wpl only a small change in reflectance remained and there were no further significant changes in lesion size between 3 and 15 wpl (Fig. 3, Supplementary Material S2, Tukey-Kramer HSD test). The area of each lesion measured by IRDF was quantitated using ImageJ and is plotted in Figure 2B. The average lesion area measured 1 dpl was 26057 ± 621 μm^2, corresponding to a spot size diameter of 182-μm incident on the retina ($n = 95$).

Histologic correlation of in vivo imaging was performed with H&E cryosections. Immediate postlaser changes were seen on animals euthanized within 1 hour following laser application. There was tissue edema and a loss of pigment in the OS and RPE (Fig. 4, 0 dpl). Histologic changes were consistently seen 1 dpl, with disorganization of the photoreceptors from the ONL down to the RPE. There was a loss of nuclei within the ONL and an increase in nuclei found in the OS zone within the laser lesion between 1 and 10 dpl. By 2 to 3 wpl the outer retinal layers had re-established their normal lamination pattern in the majority of lesions (Fig. 4). There remained a small change in contour with uneven pigmentation seen in the RPE layer. A subtle loss of pigment granules can occasionally be seen in lesions up to 15 wpl. To ensure that we were not skipping over the older lesions (>3 wpl) on sections, we placed a new laser spot (1 dpl) adjacent to the older spots to help identify the old lesion on cryosections. The new laser lesion was obvious on sections, helping to locate the subtle changes seen in the regenerated areas (not shown).

We used TUNEL staining to look for apoptosis and found TUNEL-positive cells starting 1 dpl up to 7 to 10 dpl (Fig. 5). We performed a count of DAPI-positive cells found between the RPE and ONL, and also cells found in the inner plexiform layer (IPL; Fig. 5B). We also counted the TUNEL-positive cells in the outer/inner nuclear layers (INLs), and also between the RPE and ONL (Fig. 5B). ANOVA and Tukey-Kramer HSD tests were used to detect significant differences in cell counts between time points (Supplementary Material S3). Staining in day 1 lesions was variable, with scarce TUNEL-positive cells in some sections and abundant cells in others. Early apoptotic nuclei were concentrated near the ONL, migrating toward the OS zone by approximately 3 to 7 dpl (Fig. 5). As the lesions

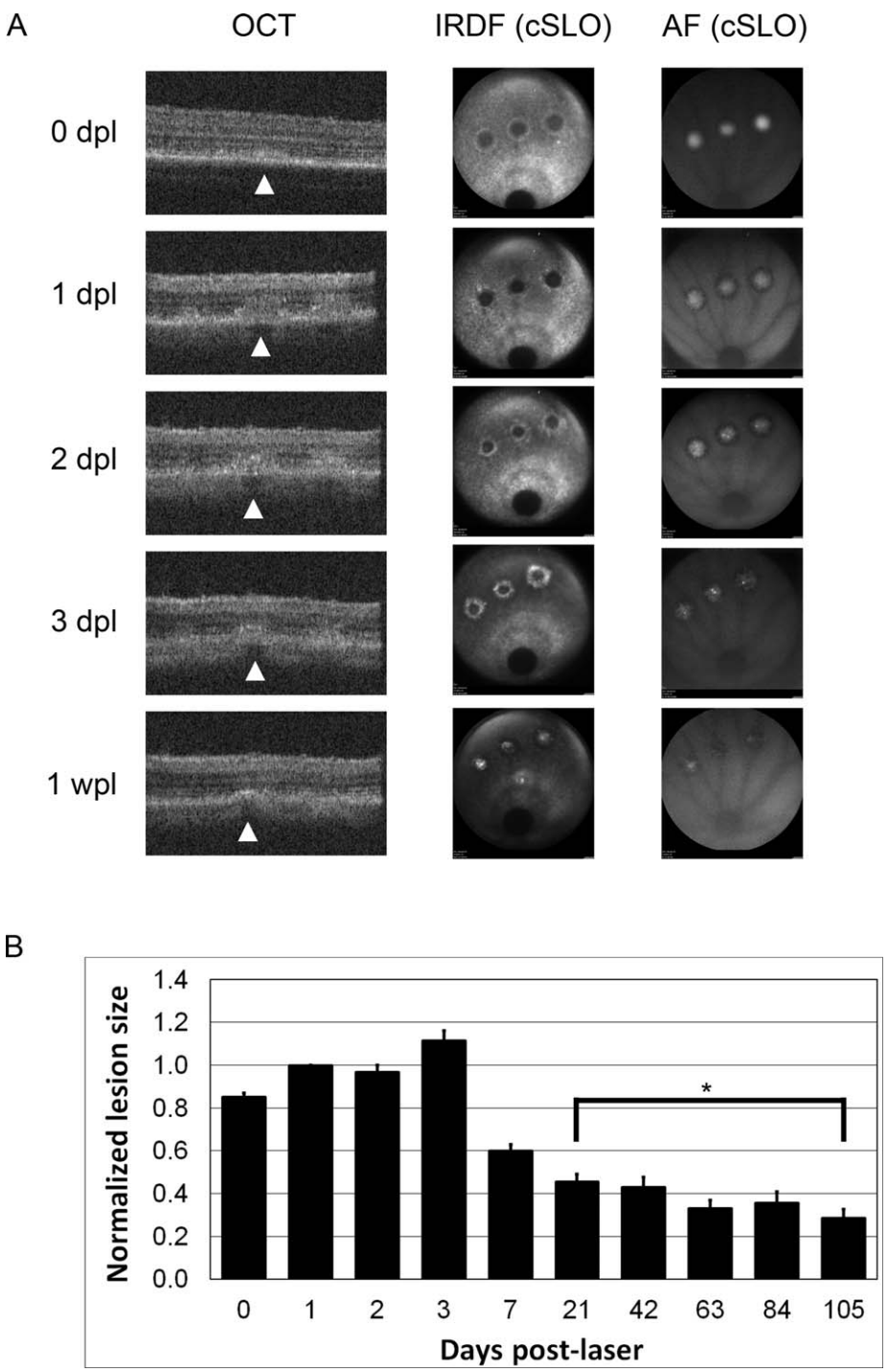

FIGURE 2. Optical coherence tomography and cSLO images of laser lesions up to 1 wpl. (**A**) Optical coherence tomography and cSLO images taken at various time points post laser lesion from a single animal. *Arrowheads* point to the central lesion on OCT. The representative B-scan images are centered on the central lesion, but all three lesions can sometimes be seen on a single B scan depending on the eye orientation (1, 2, and 3 dpl). Three discrete laser lesions can be seen on cSLO imaging. The optic nerve is visible at the bottom of each cSLO image. (**B**) Histogram of normalized lesion size measured by IRDF up to 15 wpl. *Asterisk* denotes time points without significant differences in lesion size. Total *n* for each time point: 0 dpl = 122, 1 dpl = 95, 2 dpl = 33, 3 dpl = 24, 1 wpl = 46, 3 wpl = 47, 6 wpl = 40, 9 wpl = 34, 12 wpl = 31, 15 wpl = 22.

matured, the staining was found progressively further away from the ONL and occasionally at a distant location from the lesion (Fig. 5). DAPI staining of cell nuclei showed a markedly increased number of cells migrating to the OS zone as early as 1 dpl (Fig. 5). This population of cells decreased over time until 2 wpl (Fig. 5B). In addition to this population of cells, there were also clusters of nuclei found within the IPL as early as 1 dpl in some sections (Fig. 5). These cells can also be seen on H&E-stained sections (Fig. 4). Interestingly, on several sections, the cells in the IPL persisted beyond 6 wpl (Fig. 5B), but they were always found over a previous laser lesion. The identity of these cells are not yet known.

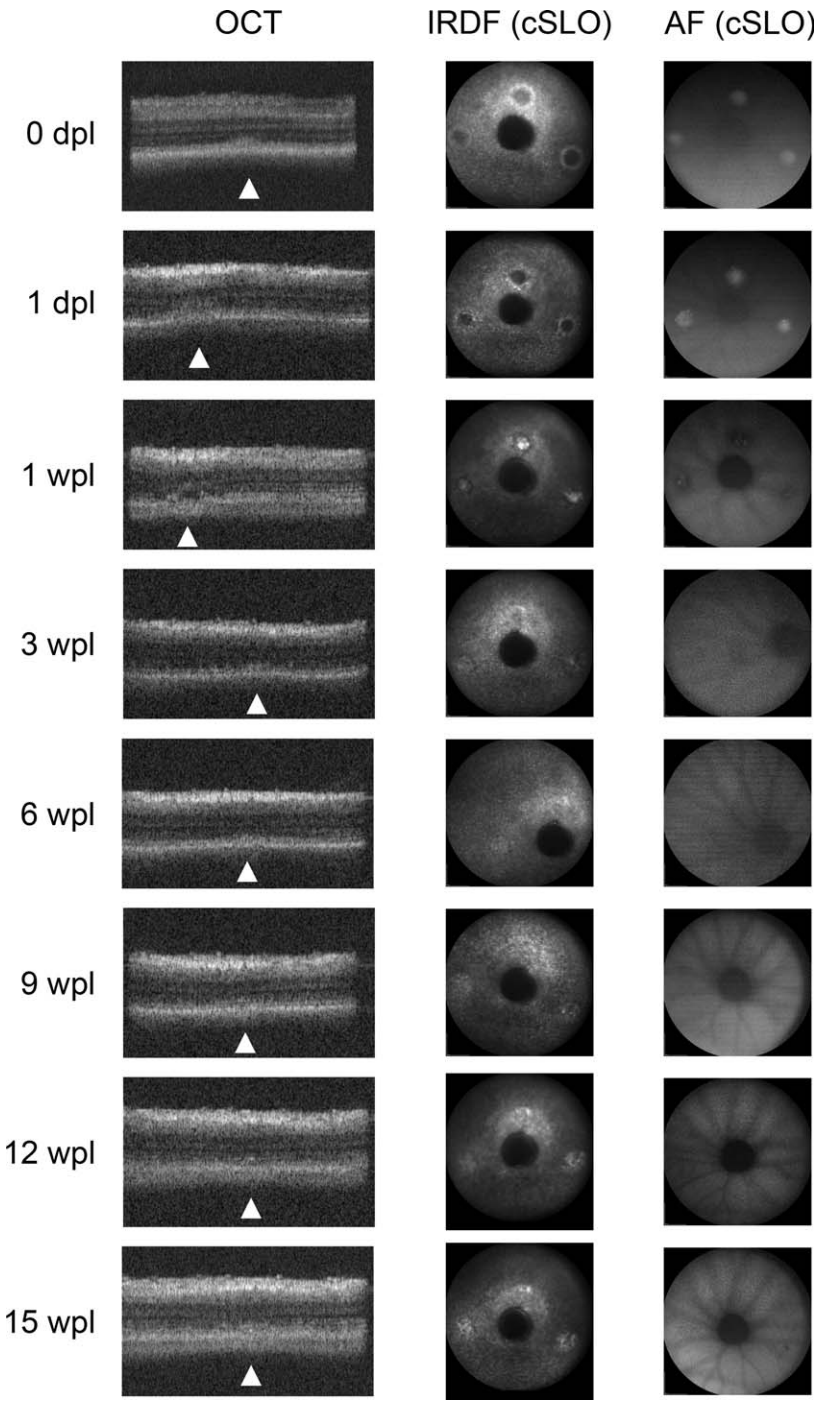

FIGURE 3. Optical coherence tomography and cSLO images taken at various time points post laser from a single animal. Optical coherence tomography and cSLO images of laser lesions 15 wpl shows regeneration and restoration of outer retinal layers. *Arrowheads* point to lesions on OCT. After 3 wpl, lesions are subtle on both OCT and cSLO.

DISCUSSION

Laser photocoagulation produced rapid and focal damage to the zebrafish retina. Under our experimental protocol, the damage was predominantly localized to the outer retina and the ONL. However, the laser parameters can be varied to produce larger areas of damage. Optical coherence tomography–guided laser photocoagulation was necessary to produce consistent lesions. Our initial attempts used a slit lamp with manual targeting of the laser. The slit-lamp method produced lesions but there was too much variability in lesion size and depth. Additionally, precise targeting to a specific area was difficult using the slit lamp. Using the C-scan image to target the lesion by OCT allowed us to precisely place each laser spot with consistent results that are less prone to operator variability. Furthermore, the actual process of laser lesion generation can be accomplished and documented in real time using the OCT B-scan capabilities (Supplementary Video S1).

Although retinal regeneration in zebrafish has been studied by a variety of methods including light damage,[1,5] cytotoxin-

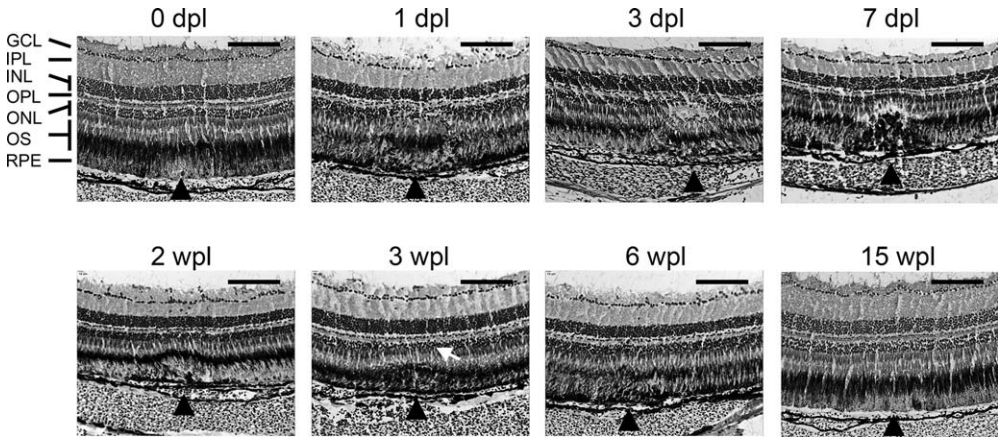

FIGURE 4. Hematoxylin and eosin–stained histosections of zebrafish retina following laser injury. Cryosections of 10 μm are shown in each panel from various time points after laser. *Scale bar*: 100 μm. *Black arrowheads* point to the location of laser lesions. A dome-shaped area of disorganization is seen between 1 dpl and 7 dpl. Relamination of the ONL occurs between 2 and 3 wpl, but with an alteration of the contour (*white arrow*). At 15 wpl, only a subtle change in pigmentation remains. GCL, ganglion cell layer; IPL, inner plexiform layer; INL, inner nuclear layer; OPL, outer plexiform layer; ONL, outer nuclear layer; OS, outer segments; RPE, retinal pigment epithelium.

mediated cell death,[2] mechanical injury,[3] and thermal injury,[4] our model offers several advantages. Optical coherence tomography–guided laser injury produced a focal lesion (average 182-μm diameter) localized to the outer retina enabling us to observe the full extent of each lesion in less than 20 histologic sections (10-μm each). Furthermore, there is minimal collateral damage with our model and the damage takes place over 300 ms, so precise timing of the regenerative response is possible with no overlapping regeneration due to prolonged exposure times.

Fundus AF following laser photocoagulation in humans and rodents reveals a characteristic pattern. Early lesions several hours old are hypo-autofluorescent. As the lesions mature, they become hyperautofluorescent and remain hyperautofluorescent with a hypo-autofluorescent rim months after injury.[12–14] In contrast, laser photocoagulation in zebrafish produced hyper-AF almost immediately with a delay of only several minutes. The pattern seen in mammals is due to damage to the lipofuscin rich RPE causing early hypo-AF, followed by a reactive change that leads to increased AF.[13] However, zebrafish do not accumulate lipofuscin in postmitotic cells,[15] and therefore would not be expected to show early hypo-AF due to RPE damage. Unlike mammals, there is very little background AF signal in zebrafish. In zebrafish, the hyperautofluorescent signal disappears at approximately 3 wpl, likely as a result of tissue regeneration.

Although IRDF imaging is not used clinically for the evaluation of retinal disease, we found it to be quite useful for monitoring regeneration in zebrafish. The increased contrast of this modality allowed us to detect changes in vivo, which would not be possible with AF in zebrafish. Unlike AF in zebrafish, which has an inherently low background signal, the IRDF image produced a consistent background image (Figs. 2, 3). When focused on the cone OSs, the cone mosaic can be visualized in this mode. Compared with AF and OCT, IRDF was able to more reliably detect subtle changes in the regenerated tissue (Fig. 3, 9–15 wpl).

As previously reported, OCT can be used to monitor regeneration in zebrafish.[5,9] Retinal damage from laser photocoagulation produced a hyperreflective band at the level of the ONL on OCT (Figs. 2, 3), which is similar to what has been reported in mammals.[16] As regeneration of the lesion ensues, the hyperreflective band disappears (Fig. 3, 6–15 wpl). The hyperreflective band seen on OCT correlated with the tissue disruption and migration of nuclei seen within the laser lesions on histologic section (Figs. 4, 5). The diffuse hyperreflective signal seen immediately following the lesion (day 0) likely represents tissue edema. The subtle hyperreflective signal seen past 3 wpl does not have an obvious histologic correlate, but may correspond to the pigmentation changes seen in the regenerated tissue or alternatively to an altered cone mosaic in the regenerated tissue.

TUNEL staining revealed apoptosis in the ONL following laser photocoagulation. In some sections, a few apoptotic cells were also seen in the INL, but the majority of apoptosis was seen in the ONL. There was a rapid reduction of apoptotic cells in the ONLs and INLs after 3 dpl, with an increasing number of apoptotic cells found in the outer segment zone (Fig. 5; Supplementary Material S3). This distribution of TUNEL+ material might suggest migration of cells that have engulfed the TUNEL+ cells, which are likely photoreceptors based on their location in the ONL. Alternatively, some of the cells that have migrated into the OS zone may undergo apoptosis. However, we cannot exclude the possibility of nonspecific labeling from the TUNEL assay, which is a known limitation.

Histologic analysis revealed a large population of cells, which migrated to the lesion site as early as 1 dpl (Figs. 4, 5). Some of these cells contained pigmented granules seen on H&E (Fig. 4) suggesting they may be cells of the macrophage or microglia lineage that have engulfed pigmented cellular debris. Future studies to identify these cells may help define the earliest signals and cellular response that follows retinal injury. In addition to this early population of cells found in the outer retinal layers, a second cluster of cells are found in the IPL (Figs. 5A, arrowheads, 5B). Interestingly, this new population of cells appear to persist beyond 6 wpl (Fig. 5B). Light induced damage in albino zebrafish resulted in proliferation of INL progenitors derived from Müller glia.[1,17] These progenitors were localized to the INL, migrating to the outer retina after light induced injury. Small nucleated cells were also found in the central and dorsal retina in light-lesioned fish in the IPL. These cells are similar in appearance to the clusters of cells that we see in our laser-lesioned fish in the IPL (Fig. 5, arrowheads). These cells are found only adjacent to each laser lesion and are not TUNEL+. Unlike the cells that migrate within the laser lesions, these cells do not appear to have pigment granules.

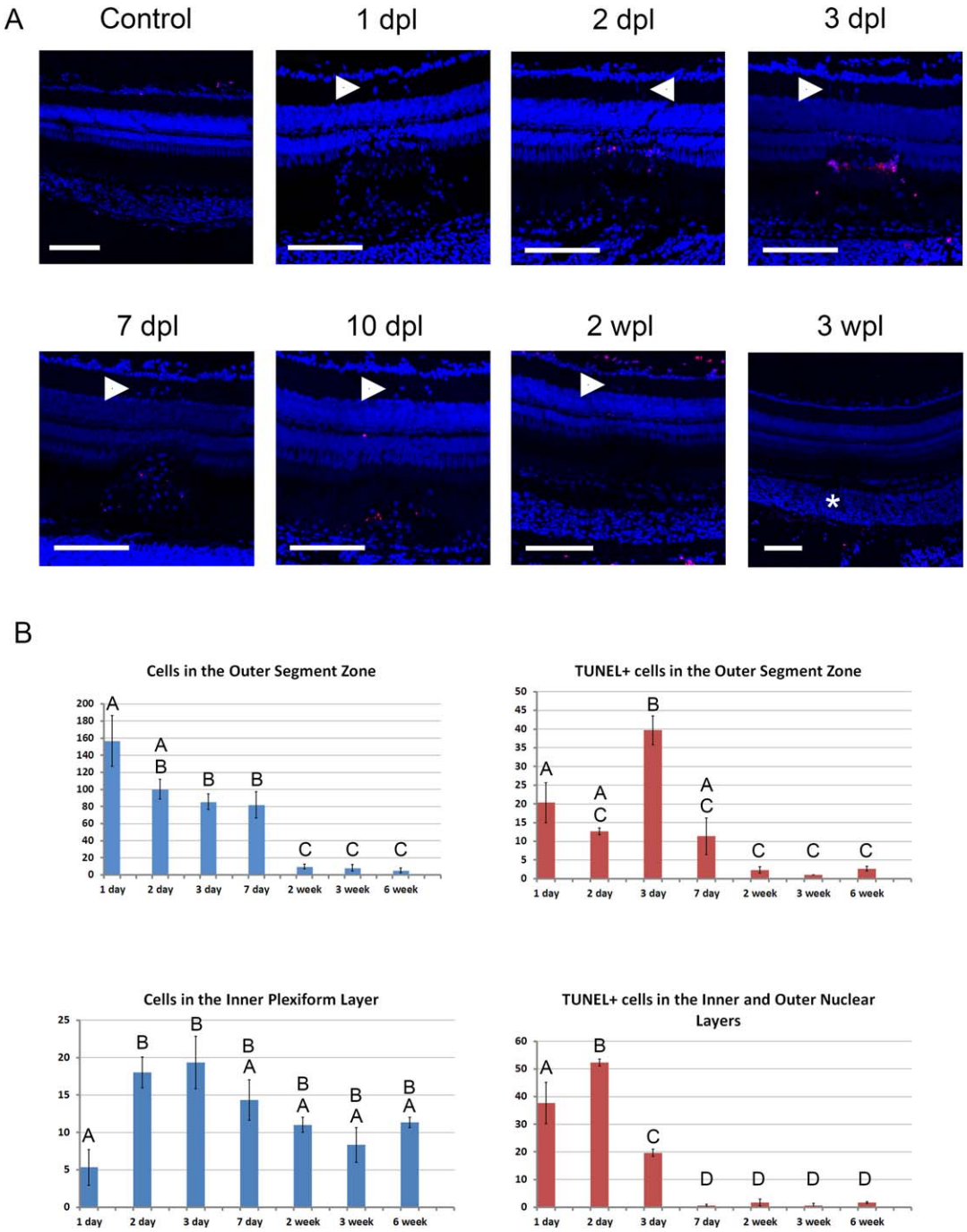

Figure 5. TUNEL and DAPI staining of zebrafish retina following laser injury. (**A**) Confocal microscopy of 10-μm cryosections are shown in each panel from various time points after laser. *Scale bar*: 100 μm. TUNEL is shown in *red* and DAPI in *blue*. The control section did not have any laser injury. *White arrowheads* point to clusters of nuclei in the IPL overlying the laser lesions. The *asterisk* shows the location of the laser lesion in the 3-wpl panel. Disorganization and loss of nuclei can be seen in the ONL between 1 and 7 dpl. The ONL is relaminated between 2 and 3 wpl. Background TUNEL labeling is seen at the outermost (scleral) surface of the retina and also at the innermost surface (control, 2 and 3 wpl). (**B**) Histograms showing distribution of DAPI- and TUNEL-positive cells following laser injury (mean ± SEM, $n = 3$ all time points). See Methods. Time points not connected by the same letter are significantly different from each other ($P < 0.05$). *Top left*: DAPI-positive cells were counted between the RPE and ONL. *Bottom left*: DAPI-positive cells within the IPL. *Top right*: TUNEL-positive cells between the RPE and ONL. *Bottom right*: TUNEL-positive cells within the INLs and ONLs.

Optical coherence tomography–guided laser photocoagulation in zebrafish is a consistent and facile method to damage the zebrafish retina. Here, we reported damage to the outer retina with little damage to other retinal layers. However, it may be possible to titrate the power to study other biological processes, for example, by damaging Bruch membrane to induce choroidal neovascularization. We believe our method has some distinct advantages. Our method produced obvious focal changes on both imaging modalities which can be used to easily monitor the regenerative progress in vivo. Previous models of retinal injury and regeneration in zebrafish induced changes to the thickness of specific retinal layers, which were

measured by OCT as a means of assessing damage and regeneration. Measurements of retinal layer thickness is a tedious process and small changes in thickness cannot be reliably detected. Our method of focal injury places damaged tissue adjacent to normal tissue allowing for the laser lesions to be more readily identified within a single OCT B scan or cSLO image. This allows for the rapid identification of regenerated retina in vivo. The use of this novel technique will allow us to further characterize the injury response, which leads to regeneration in zebrafish and scar formation and gliosis in mammals.

Acknowledgments

The authors thank Alecia Cutler, Mariya Ali, Jing Xie, Lauren Daniele, Joseph Fogerty, Emma Lessieur, Ping Song, Robert Gaivin, Minzhong Yu, George Hoppe, Suzy Yoon, and Vera Bonilha for technical assistance and creative suggestions.

Supported by National Eye Institute (Bethesda, MD, USA) Grant 1K08EY023608-01 (AY); a Research to Prevent Blindness (New York, NY, USA) unrestricted grant to Cleveland Clinic Lerner College of Medicine; a Foundation Fighting Blindness (Owings Mills, MD, USA) center grant (JGH, BAA); Research to Prevent Blindness Stein Award (BDP); and Grants R01EY020861 (BAA) and R01EY017037 (BDP).

Disclosure: **R.M. DiCicco**, None; **B.A. Bell**, None; **C. Kaul**, None; **J.G. Hollyfield**, None; **B. Anand-Apte**, None; **B.D. Perkins**, None; **Y.K. Tao**, None; **A. Yuan**, None

References

1. Vihtelic TS, Hyde DR. Light-induced rod and cone cell death and regeneration in the adult albino zebrafish (*Danio rerio*) retina. *J Neurobiol*. 2000;44:289–307.
2. Sherpa T, Fimbel SM, Mallory DE, et al. Ganglion cell regeneration following whole-retina destruction in zebrafish. *Dev Neurobiol*. 2008;68:166–181.
3. Cameron DA, Carney LH. Cell mosaic patterns in the native and regenerated inner retina of zebrafish: implications for retinal assembly. *J Comp Neurol*. 2000;416:356–367.
4. Raymond PA, Barthel LK, Bernardos RL, Perkowski JJ. Molecular characterization of retinal stem cells and their niches in adult zebrafish. *BMC Dev Biol*. 2006;6:36.
5. Weber A, Hochmann S, Cimalla P, et al. Characterization of light lesion paradigms and optical coherence tomography as tools to study adult retina regeneration in zebrafish. *PLoS One*. 2013;8:e80483.
6. Huang D, Swanson EA, Lin CP, et al. Optical coherence tomography. *Science*. 1991;254:1178–1181.
7. Rao KD, Verma Y, Patel HS, Gupta PK. Non-invasive ophthalmic imaging of adult zebrafish eye using optical coherence tomography. *Curr Sci*. 2006;90:1506–1510.
8. Kagemann L, Ishikawa H, Zou J, et al. Repeated, noninvasive, high resolution spectral domain optical coherence tomography imaging of zebrafish embryos. *Mol Vis*. 2008;14:2157–2170.
9. Bailey TJ, Davis DH, Vance JE, Hyde DR. Spectral-domain optical coherence tomography as a noninvasive method to assess damaged and regenerating adult zebrafish retinas. *Invest Ophthalmol Vis Sci*. 2012;53:3126–3138.
10. Woon WH, Fitzke FW, Bird AC, Marshall J. Confocal imaging of the fundus using a scanning laser ophthalmoscope. *Br J Ophthalmol*. 1992;76:470–474.
11. Cheng Y-H, Yu J-Y, Wu H-H, Huang B-J, Chu S-W. Spectral ophthalmoscopy based on supercontinuum. In: *Proc. SPIE 7568: Imaging, Manipulation, and Analysis of Biomolecules, Cells, and Tissues VIII, 75680I*. February 25, 2010. doi:10.1117/12.843020.
12. Boretsky A, Motamedi M, Bell B, van Kuijk F. Quantitative evaluation of retinal response to laser photocoagulation using dual-wavelength fundus autofluorescence imaging in a small animal model. *Invest Ophthalmol Vis Sci*. 2011;52:6300–6307.
13. Framme C, Brinkmann R, Birngruber R, Roider J. Autofluorescence imaging after selective RPE laser treatment in macular diseases and clinical outcome: a pilot study. *Br J Ophthalmol*. 2002;86:1099–1106.
14. Framme C, Roider J. Immediate and long-term changes of fundus autofluorescence in continuous wave laser lesions of the retina. *Ophthalmic Surg Lasers Imaging*. 2004;35:131–138.
15. Kishi S, Uchiyama J, Baughman AM, Goto T, Lin MC, Tsai SB. The zebrafish as a vertebrate model of functional aging and very gradual senescence. *Exp Gerontol*. 2003;38:777–786.
16. Koinzer S, Saeger M, Hesse C, et al. Correlation with OCT and histology of photocoagulation lesions in patients and rabbits. *Acta Ophthalmol*. 2013;91:e603–e611.
17. Vihtelic TS, Soverly JE, Kassen SC, Hyde DR. Retinal regional differences in photoreceptor cell death and regeneration in light-lesioned albino zebrafish. *Exp Eye Res*. 2006;82:558–575.

Investigative Ophthalmology & Visual Science